THE ASTRONOMICAL JOURNAL, 118:2997–3005, 1999 December

HD 62454 AND HD 68192: TWO NEW γ DORADUS VARIABLES

ANTHONY B. KAYE[1]
Applied Theoretical and Computational Physics Division, Los Alamos National Laboratory, X-TA, MS B-220, Los Alamos, NM 87545
GREGORY W. HENRY AND FRANCIS C. FEKEL[1]
Center of Excellence in Information Systems, Tennessee State University, 330 10th Avenue North, Nashville, TN 37203
RICHARD O. GRAY
Department of Physics and Astronomy, Appalachian State University, Boone, NC 28608
ELOY RODRÍGUEZ AND SUSANA MARTÍN
Instituto de Astrofísica de Andalucía, CSIC, Apdo. Postal 3004, E-18080 Granada, Spain
DOUGLAS R. GIES AND WILLIAM G. BAGNUOLO
Department of Physics and Astronomy, Georgia State University, 38 Peachtree Center Avenue, 1039-A, Atlanta, GA 30303
AND
DOUGLAS S. HALL
Dyer Observatory, Vanderbilt University, 1000 Oman Drive, Brentwood, TN 37027
Received 1999 June 29; accepted 1999 August 9

ABSTRACT

We present multilongitude, multicolor photometry and simultaneous high-resolution, high signal-to-noise spectroscopy of the newly discovered γ Doradus variables HD 62454 and HD 68192. From combined Johnson and Strömgren data, we are able to identify five independent periods in HD 62454 and two stable periods in HD 68192. The data presented are sufficient to rule out all physically meaningful types of variations, with the one exception of the high-order, low-degree, nonradial gravity-mode pulsations that are believed to be at work in γ Doradus stars. We also find that HD 62454 is a double-lined spectroscopic binary and we present an orbital solution.

Key words: stars: oscillations — stars: variables: other

1. INTRODUCTION

The search for constant comparison stars has been one of the quests of photometrists since the introduction of astronomical photometry in the early part of the 20th century. As we strive to measure stellar variability of smaller and smaller amplitudes, the constancy of comparison stars becomes increasingly important. Regions of the Hertzsprung-Russell diagram formerly assumed to contain constant stars are now known to harbor new classes of variable stars, such as the newly discovered γ Doradus variables (see Kaye et al. 1999a and references therein).

The γ Doradus stars have spectral classes clustering around F0 and luminosity classes V or IV–V. They are generally young ($\lesssim$250 Myr; see Krisciunas et al. 1995) and have solar or subsolar metallicities. Typical periods range from 0.4 to 3 days; associated amplitudes can be as large as 0.1 mag in Johnson V and several kilometers per second in radial velocity. The cause of the variations is thought to be high-order (n), low-degree (l), nonradial gravity-mode pulsations caused by convective blocking, a mechanism similar to the classical κ-effect (Guzik, Kaye, & Bradley 1999).

During the course of a program to monitor light variability in solar-type stars (Henry 1999), a number of comparison stars around spectral type F0 V, including HD 62454 and HD 68192, were found to be low-amplitude variables and, thus, good candidates to exhibit γ Doradus type variability. In this paper, we investigate in detail recent multilongitude, multicolor differential photometry and simultaneous high-resolution, high signal-to-noise spectroscopy of these two newly discovered variable stars. We also show that HD 62454 is a double-lined spectroscopic binary star and present an orbital solution.

2. OBSERVATIONS

Time-series analysis of γ Doradus stars can be quite difficult when only single-site data are available. This is mainly because the periods of variation in both the photometry and the spectroscopy are often close to 1 day. We attempted to alleviate this aliasing problem (to some extent) by utilizing multisite photometry.

2.1. *Photometry*

We acquired Johnson and Strömgren photometry with two automatic photoelectric telescopes (APTs) located at Fairborn Observatory, Washington Camp, Arizona. We obtained additional Strömgren photometry with the 0.9 m telescope at the Sierra Nevada Observatory in Spain. The observations from these three telescopes are described below and summarized in Table 1 for HD 62454 and Table 2 for HD 68192. We analyzed the V, B, y, and combined $V+y$ data sets for each star.

2.1.1. *APTs*

A 0.4 m APT at Fairborn Observatory acquired differential BV photometry of both stars during the 1997–1998 observing season. Each differential magnitude obtained with this telescope is the mean of three intercomparisons between the variable star and a constant comparison star in the sense of variable minus comparison. The comparison star for HD 62454 is HD 65664 ($V = 7.27$, F5); the comparison for HD 68192 is HD 70312 ($V = 7.5$, F5). Mean

[1] Visiting Astronomer, Kitt Peak National Observatory, National Optical Astronomy Observatories, operated by the Association of Universities for Research in Astronomy, Inc., under cooperative agreement with the National Science Foundation.

TABLE 1

HD 62454: PHOTOMETRIC AND SPECTROSCOPIC OBSERVATIONS

Telescope Aperture (m)	Location	Observation Type	n	Date Range HJD − 2,400,000
0.4	Arizona	V photometry	438	50,718.96–50,949.63
		B photometry	446	50,718.96–50,949.63
0.9	Spain	*uvby* photometry	21	50,734.53–50,735.66
		uvby photometry	23	50,833.60–50,852.39
0.9	Arizona	Blue spectra	33	50,777.96–50,787.98
		Red spectra	3	51,095.01, 51,303.67, 51,304.68
		Yellow spectra	2	51,260.63, 51,262.65
0.8	North Carolina	Classification spectrum	1	51260.50

differential magnitudes with internal standard deviations greater than 0.01 mag were rejected from the analysis to filter observations taken under nonphotometric conditions. The observations were corrected for differential atmospheric extinction and transformed to the Johnson UBV system. Multiple observations were obtained each night whenever possible at hour angles of -4, -2, 0, $+2$, and $+4$. Check-star observations demonstrated that both comparison stars were constant to 0.0035 mag, the limit of precision for this APT. Further details on the 0.4 m APT as well as on the observing and data reduction procedures can be found in Henry (1995).

A 0.75 m APT at Fairborn obtained additional Strömgren *by* photometry of HD 68192 during the 1993–1994, 1994–1995, and 1995–1996 observing seasons. One observation was made each clear night with the same comparison star as the 0.4 m APT; each observation represents the mean of three differential observations of the variable and comparison stars. These observations were also corrected for differential extinction, then transformed to the Strömgren system. Nightly mean differential magnitudes were rejected if their internal standard deviations were greater than 0.005 mag. The precision of a single observation with this telescope is typically about 0.0014 mag. Because the mean of the 249 Strömgren y differential magnitudes from the 0.75 m APT was 0.0017 mag fainter than the mean of the 425 Johnson V differential magnitudes from the 0.4 m APT, a correction of -0.0017 mag was added to the Strömgren y data to bring them into line with the Johnson V data. Further details on the operation of the 0.75 m APT can be found in Henry (1999).

2.1.2. *Sierra Nevada*

We also used the 0.9 m telescope and six-channel *uvbyβ* photometer at the Sierra Nevada Observatory to make further differential Strömgren *uvby* observations of both stars during 1997 October and 1998 January. The photometer uses uncooled EMI 9789QA photomultipliers for simultaneous measurements in each band. The comparison stars were the same ones used by the APTs at Washington Camp. Some observations from Sierra Nevada overlapped in time with observations from the 0.4 m APT in Arizona. We used these overlapping observations to slide the Strömgren y differential magnitudes from Sierra Nevada into agreement with the Johnson V observations from the APT. Adjustments of -0.003 mag and $+0.0132$ mag were applied to the 1997 October and 1998 January data, respectively, on HD 62454 to bring them into line with the 0.4 m APT data. We do not understand the particular physical or engineering difficulties which necessitate two different corrections, one for each observing run, in this star. Nonetheless, since the correlation between the Sierra Nevada data and the APT data is good in the region of overlap between the two data sets, we have some confidence in our procedure. No adjustments were necessary for the HD 68192 observations. This may be due to the fact that the color difference between the comparison and variable stars was much smaller for HD 68192 (0.08 mag) than for HD 62454 (0.20 mag).

2.2. *Spectroscopy*

2.2.1. *Kitt Peak National Observatory*

Over 11 nights during 1997 December, we obtained 33 high-resolution, high signal-to-noise spectra of HD 62454 and 31 of HD 68192 with the 0.9 m coudé feed telescope and spectrograph. We took those spectra simultaneously with the photometric observations obtained at Washington Camp, Arizona, and contemporaneously with the photometry from Sierra Nevada, Spain.

TABLE 2

HD 68192: PHOTOMETRIC AND SPECTROSCOPIC OBSERVATIONS

Telescope Aperture (m)	Location	Observation Type	n	Date Range HJD − 2,400,000
0.8	Arizona	y photometry	91	49,277.00–49,482.65
		y photometry	85	49,639.01–49,840.66
		y photometry	73	50,013.01–50,214.65
0.4	Arizona	V photometry	425	50,714.99–50,965.64
		B photometry	432	50,714.99–50,965.64
0.9	Spain	*uvby* photometry	21	50,734.54–50,735.68
		uvby photometry	23	50,833.61–50,852.41
0.9	Arizona	Blue spectra	31	50,777.82–50,788.77
		Yellow spectra	2	51,260.65, 51,262.67
0.8	North Carolina	Classification spectrum	1	51,260.50

Each of these spectra covers the blue-wavelength region 4403 to 4617 Å, has a resolution of 0.18 Å, and was obtained with grating A in third order, camera 5, and the long collimator. Filter 4-96 was used to block competing orders. Data were recorded on the F3KB CCD (3000 × 1000 pixels, 15 × 15 μm pixel size, 75% DQE at 4210 Å). A typical exposure time in this region was 1800 s, resulting in a signal-to-noise ratio of approximately 300. ThAr exposures used for wavelength calibration were taken immediately before and after each stellar exposure.

In addition, we obtained three red-wavelength spectra of HD 62454 at KPNO (one during 1998 October and two during 1999 May) with the coudé feed telescope, coudé spectrograph, grating A, camera 5, and a Texas Instruments CCD. The spectra are centered at 6430 Å and have a wavelength range of over 80 Å and a resolution of 0.21 Å.

During 1999 March at KPNO, we also acquired two yellow-wavelength spectra of each star with the coudé feed telescope, coudé spectrograph, grating A, camera 5, and the F3KB CCD. These spectra cover the wavelength region between 5850 and 6150 Å and have a resolution of 0.21 Å.

All these KPNO spectra were reduced at the NOAO offices in Tucson, Arizona, with IRAF.[2] After optimal aperture extraction, bias subtraction, and flat-field division, we rectified the spectra to a unit continuum by fitting a straight line through known continuum regions. Since the blue-wavelength spectra were obtained to search primarily for line-profile variations, the spectra were put on a uniform heliocentric wavelength grid to place the absorption features of each spectrum at the same wavelength. The yellow- and red-wavelength spectra were obtained to improve the preliminary orbital elements, and so a rest-wavelength solution was applied to those spectra.

Depending on the type of wavelength solution, different radial velocity measurement techniques were used by the different observers. Past experience indicates that the various techniques used produce velocities that can be combined into a single data set.

2.2.2. *Dark Sky Observatory*

In addition to the KPNO spectra, one classification resolution spectrum of both HD 62454 and HD 68192 was acquired with the Gray/Miller Cassegrain spectrograph on the 0.8 m telescope at the Dark Sky Observatory at Appalachian State University. These classification spectra were obtained with a 1200 lines mm^{-1} grating in first order and a Texas Instruments 1024 × 1024 thinned, back-illuminated CCD. Each spectrum has a range of 800 Å centered on 4200 Å, a 2 pixel resolution of 1.8 Å, and a signal-to-noise ratio in excess of 300.

All spectra are summarized in Table 1 for HD 62454 and Table 2 for HD 68192.

3. HD 62454

3.1. *Basic Properties*

One of us (R. O. G.) has devised a technique (see Gray, Graham, & Hoyt 1999 for details) that utilizes a multidimensional simplex method to fit the basic parameters of a star ($T_{\rm eff}$, $\log g$, ξ_t, and [M/H]) by iteratively choosing the model that best matches the observed classification spectrum *and* the fluxes from Strömgren *uvby* photometry. The synthetic spectra used in this technique were computed with the program SPECTRUM and the ATLAS9 models of Kurucz (1993). The conversion from *uvby* photometry to fluxes was carried out with the formulae of Gray (1998).

HD 62454 is a double-lined spectroscopic binary with a mass ratio of 1.34 ± 0.02 (see § 3.3 and Table 6). This complicates the derivation of the basic properties of this star. A straightforward application of the multidimensional simplex method yields $T_{\rm eff} = 7120$ K, $\log g = 4.21$, and $\xi_t = 2.94$ km s^{-1} for the composite spectrum of HD 62454. To find the basic parameters of the two component stars, we first found the combined luminosity, $8.62 \pm 0.16\ L_\odot$, from the absolute magnitude and the bolometric correction (0.03; Flower 1996). From the $\log g$ of the above fit, we assumed that the stars are on the main sequence, and thus the mass-luminosity relationship is applicable. We used the mass-luminosity and the mass-radius relationships of Gorda & Svechnikov (1998) to derive iteratively the individual masses ($M_A = 1.52 \pm 0.20\ M_\odot$ and $M_B = 1.14 \pm 0.20\ M_\odot$), as well as the individual radii ($R_A = 1.64 \pm 0.14\ R_\odot$ and $R_B = 1.36 \pm 0.14\ R_\odot$). The mass-luminosity relationship then yielded $L_A = 6.44 \pm 0.20\ L_\odot$ and $L_B = 2.18 \pm 0.20\ L_\odot$. The Stephan-Boltzmann law can be used to derive the effective temperature for the individual components; we found the temperature of the primary star to be $T_{\rm eff} = 7190 \pm 300$ K, and the secondary star $T_{\rm eff} = 6020 \pm 300$ K. The masses and radii can be used to find the individual gravities. For the primary, $\log g = 4.19 \pm 0.09$; for the secondary, $\log g = 4.23 \pm 0.09$. These effective temperatures and gravities nicely bracket the multidimensional simplex solution for the composite spectrum. To check this solution, we have calculated, using the ATLAS9 program of Kurucz (1993), fluxes for the models $T_{\rm eff} = 7200$ K, $\log g = 4.2$, and $\xi_t = 2.0$ km s^{-1} and $T_{\rm eff} = 6000$ K, $\log g = 4.2$, and $\xi_t = 2.0$ km s^{-1}. These fluxes have been normalized to unity at the effective wavelength of the Johnson V band, and then the 6000 K model fluxes were added to the 7200 K model fluxes multiplied by a factor of 3.25 (the ratio of the luminosities in the V band of the two stars in the system). We then converted the theoretical fluxes to absolute fluxes using the absolute flux in the Johnson V band. Figure 1 compares the resulting energy distribution with fluxes from Strömgren photometry and the *TD-1* satellite. While the fluxes in the Strömgren

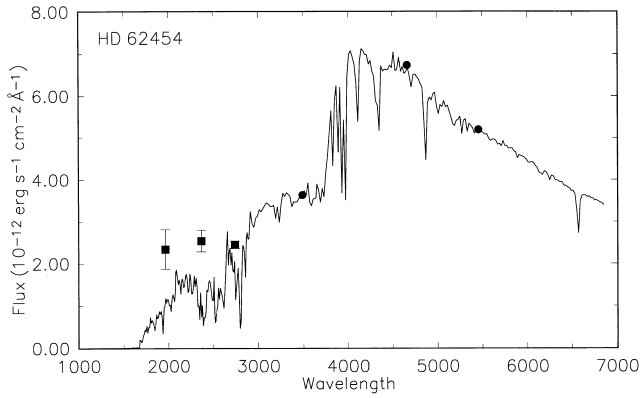

FIG. 1.—Comparison of the observed fluxes of HD 62454 with the theoretical model composed of a 7200 K, $\log g = 4.2$ model and a 6000 K, $\log g = 4.2$ model calculated with the ATLAS9 stellar atmospheres program (Kurucz 1993): *circles*, Strömgren *uby* photometry; *squares*, *TD-1* satellite fluxes. These models have been scaled and added as described in the text. The two shortest wavelength flux points from the *TD-1* satellite appear to show an excess UV flux, possibly pointing to the presence of a low-luminosity, hot companion.

[2] IRAF is distributed by the National Optical Astronomy Observatories.

bands and the 2740 Å *TD-1* band are in good agreement with the theoretical fluxes, the two short-wavelength bands of the *TD-1*satellite show an excess flux. These cannot be brought into agreement with the theoretical fluxes for any reasonable combination of models. We do not place much weight on this discrepancy, as the fluxes in these bands are quite low (and have large error bars), but we cannot exclude the possibility that there may be a hot white dwarf tertiary star in this system.

We determined the spectral types of both components of HD 62454 by visually comparing their red-wavelength spectra to spectra of F stars (Fekel 1997) that had well determined spectral types by reliable classifiers. The standards were obtained in the 6430 Å region with the same telescope, spectrograph, and detector setup. Lines from both components are seen at red wavelengths, making classification somewhat more difficult. Nevertheless, we classify the primary as F1 V and the secondary as F8 V. According to the spectral type versus temperature relation given by Gray (1992), we find $T_{\rm eff} = 6826$ K for the primary and 6115 K for the secondary. A one-subclass uncertainty for the spectral type makes the assumed effective temperatures well within the 1 σ error bars of the calculated effective temperatures given above.

Using the procedure and empirical relation of Fekel (1997) and macroturbulences of 5 and 3 km s^{-1} for the primary and secondary, respectively, we determine $v \sin i = 11.5 \pm 1.0$ km s^{-1} for the primary and 5.0 ± 1.0 km s^{-1} for the secondary.

The basic properties of HD 62454 are summarized in Table 3.

3.2. *Photometric Results*

We used the least-squares method of Vaniĉek (1971) to search for periodicities in the photometric data. This technique searches for multiple periods in the low-frequency domain without prewhitening, thus avoiding the dangers associated with other techniques. This method has been used in the data analysis of various other γ Doradus stars, most recently for HR 8799 (Zerbi et al. 1999) and HR 8330 (Kaye et al. 1999b).

Table 4 presents the results of our frequency analysis of the 482 $V + y$ and 446 B photometric measurements. Column (1) lists the photometric bandpass. Column (2) lists the number of observations. Columns (3) and (4) list the periods and corresponding frequencies found. Column (5) lists the peak-to-peak amplitude. Column (6) lists T_p, a time of photometric minimum light near the middle of the data set, assuming each periodicity can be modeled as a pure sine curve.

Figure 2 shows the least-squares spectra of the $V + y$ data set of HD 62454 showing the peaks corresponding to the five periodic signals and their aliases. All five frequencies were confirmed within their errors in the B data set. The B amplitudes are $\sim$30% larger than the $V + y$ amplitudes. We note for completeness that a possible signal near 2.9 day^{-1} and its aliases shown in the bottom panel was not confirmed in the B data set and so is not included in Table 4. The final residuals in the $V + y$ data set reached 0.005 mag; the residuals above and beyond the instrumental limit may be indicative of other small-amplitude periodicities or of instability (i.e., amplitude and/or phase variations) within the reported signals over the course of these observations. Future observations will be required to resolve this point.

The five panels in Figure 3 plot the $V + y$ data phased with the five confirmed frequencies. No prewhitening has been performed in any of the panels. Phase 0.0 in each panel corresponds to a time of photometric minimum, T_p, for each frequency given in Table 4.

3.3. *Spectroscopic Results*

Kaye (1998a) showed HD 62454 to be a spectroscopic binary. Although lines of both components are visible in our spectra, our derived properties indicate that only the primary is likely to be a γ Doradus variable. To search for pulsation-related line-profile variations in the primary component, we needed to remove the secondary spectral component and to reregister the primary spectra by removing the binary motion.

For the 33 KPNO blue-wavelength spectra, we first measured radial velocities for both components using the cross-correlation function (CCF) method described by Penny,

TABLE 3

HD 62454: Basic Properties

Quantity	Composite	Primary Component	Secondary Component	Reference
Observed quantities:				
$b-y$	0.214 ± 0.003	...	...	1
m_1	0.185 ± 0.004	...	...	1
c_1	0.619 ± 0.004	...	...	1
$B-V$	0.364 ± 0.015	...	...	2
$v \sin i$ (km s^{-1})	...	11.5 ± 1.0	5.0 ± 1.0	3
π (mas)	11.18 ± 1.01	...	...	2
Derived quantities:				
$T_{\rm eff}$ (K)	7120	7190 ± 300	6020 ± 300	3
[M/H]	0.16 ± 0.10	...	...	4
$\log g$	4.21	4.19 ± 0.09	4.23 ± 0.09	3
ξ_t (km s^{-1})	2.94	...	...	3
$M_{\rm bol}$	2.41 ± 0.02	2.73 ± 0.04	3.90 ± 0.04	3
M ($M_\odot$)	...	1.52 ± 0.20	1.14 ± 0.20	3
R ($R_\odot$)	...	1.64 ± 0.14	1.36 ± 0.14	3
L($L_\odot$)	8.62 ± 0.16	6.44 ± 0.20	2.18 ± 0.20	3
Spectral type	...	F1 V	F8 V	3

References.—(1) Olsen 1983; (2) ESA 1997; (3) this paper; (4) Kaye et al. 1999a.

TABLE 4

HD 62454: Results from Photometric Data

Photometric Band(s) (1)	n (2)	Period (days) (3)	Frequency (day^{-1}) (4)	Amplitude[a] (mmag) (5)	T_p (HJD − 2,400,000) (6)
$V+y$	482	0.62443 ± 0.00005	1.60146 ± 0.00012	12.45 ± 0.57	50,830.062 ± 0.009
		0.69600 ± 0.00014	1.43678 ± 0.00029	11.26 ± 0.58	50,829.906 ± 0.011
		0.57580 ± 0.00003	1.73671 ± 0.00010	10.46 ± 0.58	50,830.113 ± 0.011
		0.54534 ± 0.00013	1.83372 ± 0.00044	7.4 ± 0.6	50,829.633 ± 0.015
		0.55324 ± 0.00016	1.80753 ± 0.00054	6.6 ± 0.6	50,829.727 ± 0.017
B	446	0.62447 ± 0.00008	1.60136 ± 0.00021	15.56 ± 0.78	50,830.059 ± 0.010
		0.69602 ± 0.00009	1.43674 ± 0.00019	15.09 ± 0.79	50,829.902 ± 0.012
		0.57589 ± 0.00009	1.73644 ± 0.00028	13.81 ± 0.79	50,830.121 ± 0.011
		0.54534 ± 0.00012	1.83372 ± 0.00040	10.3 ± 0.8	50,829.633 ± 0.014
		0.55322 ± 0.00016	1.80760 ± 0.00052	9.0 ± 0.8	50,829.738 ± 0.016

[a] The amplitudes of variability, which we assume arises from the brighter F1 V component, have not been corrected for dilution from the F8 V secondary. To convert to intrinsic amplitudes of the F1 V primary, the $V+y$ amplitudes must be multiplied by 1.31 and the B amplitudes must be multiplied by 1.21.

Gies, & Bagnuolo (1997). We selected the single-lined spectrum obtained at HJD 2,450,781.952 as a reference spectrum and then cross-correlated each individual spectrum with this reference spectrum. We fitted single Gaussians to the primary and secondary signals in CCFs for where the profiles were well separated, and we used the average widths (standard deviations of 0.208 and 0.175 Å for the primary and secondary, respectively) and peak intensity ratio (0.21) to make a constrained double-Gaussian fit of each composite CCF (where we solve for only the position of each peak and the overall normalization). The resulting velocities were transformed to an absolute scale by adding +7.8 km s^{-1}, the radial velocity found by fitting parabolae to the lower halves of the lines Fe II λ4508.289 and Ti II λ4501.278 in the reference spectrum.

We determined velocities of the Na D region observations (the yellow spectra in Table 1) with the IRAF routine RVIDLINES. Each velocity is the mean of the measurement of about 16 individual lines, including the two Na

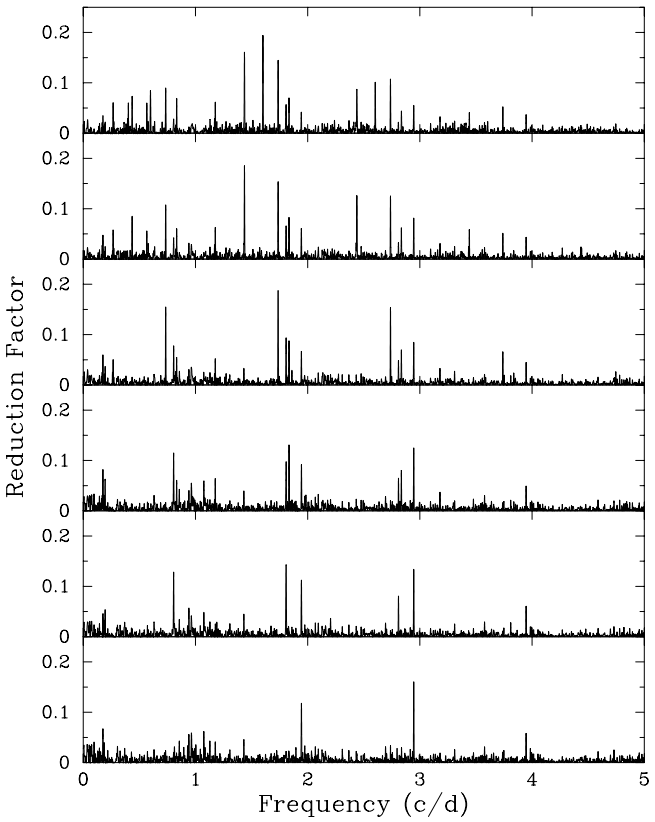

Fig. 2.—Least-squares spectra of the complete HD 62454 $V+y$ data set, showing the progressive removal of known constituents. *Top*, no signals removed; *second*, only the $\nu = 1.601$ day^{-1} signal removed; *third*, the $\nu = 1.437$ day^{-1} signal has also been removed; *fourth*, the $\nu = 1.737$ day^{-1} signal has also been removed; *fifth*, the $\nu = 1.834$ day^{-1} signal has also been removed; *bottom*, the $\nu = 1.808$ day^{-1} signal has also been removed. All five frequencies were confirmed in the B data set. A possible sixth signal, at $\nu \approx 2.9$ day^{-1}, and its aliases remain in the bottom panel, but this frequency was not confirmed in the B data set and so is not listed in Table 4.

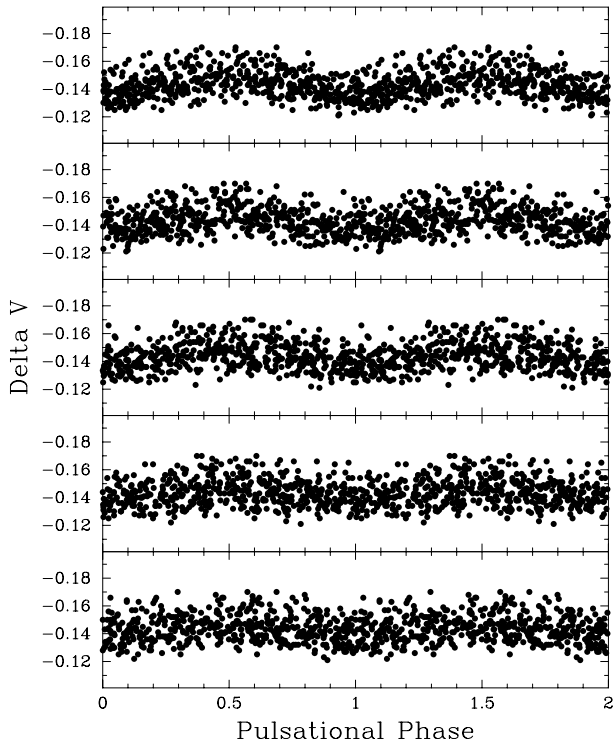

Fig. 3.—The $V+y$ photometric data for HD 62454, phased with the five independent frequencies and times of minimum from Table 4. Frequencies (*top to bottom*): 1.60146, 1.43678, 1.73671, 1.83372, and 1.80753 day^{-1}. No prewhitening has been performed in any of the panels. All panels are plotted on the same scale.

D lines and more than a dozen Fe I lines. We measured radial velocities of the 6430 Å spectra with the IRAF cross-correlation routine FXCOR. IAU standard-star velocities were assumed from Scarfe, Batten, & Fletcher (1990).

Kaye (1998a) analyzed the eight nights of data obtained in 1997 December, which span 11 days, and found a period of 14.05 days. Our set of velocities now covers 326 days. Period searches of the primary and secondary velocities resulted in a best period of 11.615 days in each case and indicate that the 14.05 day period is not viable. We obtained separate orbital solutions for the primary and secondary velocities with a differential corrections program, called SB1, of Barker, Evans, & Laing (1967). We assigned zero weight to all velocities of blended components that were within 5 km s^{-1} of the center-of-mass velocity. From a comparison of the two solutions, we gave weights of 0.2 to the remaining secondary velocities relative to those of the primary. We then determined a two-component orbital solution for the complete data set (Table 5), whose elements are listed in Table 6. Figure 4 shows the velocities and the computed orbit. Comparison of our results with the preliminary elements of Kaye (1998a) shows significant differences. Because of the increased time span of the data and the orbital solution of both components, our elements supersede those of Kaye (1998a).

TABLE 5

HD 62454: RADIAL VELOCITIES

HJD (2,400,000+)	Orbital Phase	V_p (km s^{-1})	$O-C_p$ (km s^{-1})	V_s (km s^{-1})	$O-C_s$ (km s^{-1})
50,777.957.....	0.187	55.2	0.5	−56.0	−1.1
50,777.978.....	0.189	55.7	1.0	−56.2	−1.2
50,778.851.....	0.264	52.4	−0.6	−53.4	−0.7
50,778.873.....	0.266	51.9	−1.0	−53.3	−0.8
50,778.961.....	0.274	50.8	−1.4	−52.2	−0.5
50,778.983.....	0.276	50.8	−1.2	−51.7	−0.3
50,780.764.....	0.429	29.2	0.0	−21.8	−0.9
50,780.785.....	0.431	29.5	0.6	−21.9	−1.5
50,780.806.....	0.433	29.2	0.7	−21.4	−1.4
50,780.879.....	0.439	28.0	0.6	−19.3	−0.9
50,780.900.....	0.441	27.7	0.7	−19.0	−1.1
50,780.921.....	0.443	27.2	0.5	−18.2	−0.7
50,781.743.....	0.513	11.7	−1.0	6.0	4.8
50,781.790.....	0.518	9.3	−2.6	12.3	10.0
50,781.885.....	0.526	8.1	−2.1	10.2	5.7
50,781.952.....	0.531	7.7	−1.4	7.8	1.7
50,781.998.....	0.535	6.9	−1.3	7.6	0.4
50,782.773.....	0.602	−6.8	−1.1	26.6	0.7
50,782.996.....	0.621	−9.8	0.0	34.0	2.7
50,785.878.....	0.869	−42.7	0.5	77.1	1.1
50,785.899.....	0.871	−42.5	0.6	77.1	1.3
50,785.920.....	0.873	−42.3	0.6	77.0	1.3
50,786.008.....	0.881	−42.3	−0.1	76.0	1.3
50,786.029.....	0.882	−42.2	−0.1	76.0	1.5
50,786.891.....	0.957	−23.1	0.4	45.6	−4.0
50,786.912.....	0.958	−22.7	0.0	45.1	−3.5
50,786.978.....	0.964	−21.2	−0.8	42.7	−2.8
50,787.034.....	0.969	−19.7	−1.3	41.5	−1.4
50,787.752.....	0.031	8.5	−2.5	10.5	7.0
50,787.852.....	0.039	15.8	0.6	3.1	5.2
50,787.873.....	0.041	17.2	1.2	1.4	4.6
50,787.955.....	0.048	20.9	1.6	−1.7	5.9
50,787.976.....	0.050	21.4	1.3	−3.0	5.7
51,095.013.....	0.485	17.6	−0.8	−6.8	−0.4
51,260.627.....	0.744	−33.4	0.4	61.7	−1.7
51,262.650.....	0.918	−37.7	−2.0	63.4	−2.6
51,303.668.....	0.450	23.3	−2.0	−16.6	−0.9
51,304.676.....	0.537	6.6	−1.4	6.6	−0.9

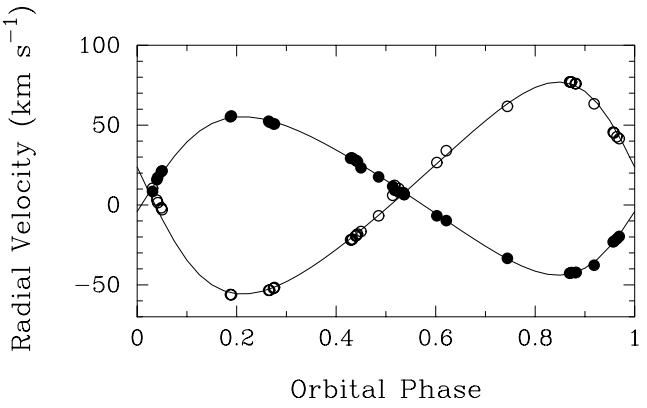

FIG. 4.—Radial velocities for the primary (*filled circles*) and secondary (*open circles*) components of HD 62454. Lines illustrate the final double-lined orbital solution having $P = 11.6147$ days. Zero phase is the time of periastron passage.

We next used the Doppler tomography algorithm to reconstruct the average primary and secondary blue-wavelength spectra (Bagnuolo et al. 1994). We adopted the measured radial velocities for the input Doppler shifts of each component, and we assumed a continuum flux ratio of $f_s/f_p = 0.21$ (the adopted intensity ratio used in the double-Gaussian fits of the CCFs). We made 100 iterations using a damping factor of 0.8, and we took the reference (single-lined) spectrum as our initial estimate for each component (none of these input parameters are critical for the final reconstructions). The reconstructed secondary spectrum is clearly of a later type with stronger Fe I lines and weaker Fe II lines than those in the primary's spectrum. We then shifted the reconstructed secondary spectrum to the measured Doppler shift of each observed spectrum and subtracted it. The resulting spectra of the primary alone were renormalized to a unit continuum and then shifted according to the orbital fit discussed above. This final sequence of primary spectra was the input for our standard time-series analysis methods to investigate the profile variations caused by pulsation.

Once we removed the binary motion and the contribution of the secondary star from the spectra, we searched for

TABLE 6

HD 62454: ORBITAL ELEMENTS

Element	Value
P (days)	11.6147 ± 0.0014
T_{per} (HJD) (days).....	2,451,310.06 ± 0.04
K_A (km s^{-1})	46.6 ± 0.3
K_B (km s^{-1})	66.4 ± 0.7
e	0.217 ± 0.005
ω_A (deg).....	258.6 ± 1.4
ω_B(deg).....	78.6 ± 1.4
γ (km s^{-1})	7.8 ± 0.2
M_A/M_B.....	1.34 ± 0.02
$M_A \sin^3 i$.....	1.00 ± 0.02
$M_B \sin^3 i$.....	0.75 ± 0.01
$a_A v \sin i$ (10^6 km).....	7.74 ± 0.05
$a_B v \sin i$ (10^6 km).....	10.35 ± 0.11
σ (km s^{-1})	1.1

other periodic signals. To do this, we calculated the moments of the Fe II λ4508.289 line (see, e.g., Balona 1987) and performed a time-series analysis on these data using the method of Vaniček (1971). Convincing periodicities were not found, presumably because of several factors, including the small number of observations, complications resulting from the double-lined nature of the system, the uncertainties of the orbital elements, and uncertainties in the velocity measurements.

4. HD 68192

4.1. *Basic Properties*

Using the classification spectrum obtained for HD 68192 at the Dark Sky Observatory and Strömgren *uvby* photometry from Olsen (1983), we have derived the following parameters for this star: $T_{\rm eff} = 6920$ K, [M/H] = 0.021, $\log g = 3.87$, and $\xi_t = 1.8$ km s^{-1}. These parameters and their estimated errors may be found in Table 7.

Estimates for the radius of this star may be computed in two ways. First, the $B-V$ color index (Table 7) may be used to derive a visual surface brightness parameter that is well correlated with the angular diameter (Barnes, Evans, & Moffett 1978). The angular diameter, combined with the *Hipparcos* parallax of 10.67 ± 0.81 mas (ESA 1997) yields $R = 2.13 \pm 0.06\ R_\odot$. On the other hand, the $T_{\rm eff}$ from the model fit may be used in conjunction with the absolute visual magnitude and the bolometric correction (0.03; Flower 1996) to derive $R = 2.14 \pm 0.05\ R_\odot$. We adopt the weighted mean as our "final" radius value: $R = 2.14 \pm 0.05\ R_\odot$. With the previously determined $\log g = 3.87 \pm 0.05$, this radius yields a mass of $M = 1.23 \pm 0.15\ M_\odot$.

TABLE 7

HD 68192: Basic Properties

Quantity	Value	Reference
Observed Quantities:		
$b-y$	0.227 ± 0.003	1
m_1	0.169 ± 0.004	1
c_1	0.647 ± 0.004	1
$B-V$	0.363 ± 0.009	2
$v \sin i$ (km s^{-1})	85 ± 5	3
π (mas)	10.67 ± 0.81	2
V_r (km s^{-1})	27.0 ± 0.05	4
Derived Quantities:		
$T_{\rm eff}$ (K)	6920 ± 75	4
[M/H]	0.021 ± 0.10	4
$\log g$	3.87 ± 0.05	4
ξ_t (km s^{-1})	1.8 ± 0.5	4
M_V	2.29 ± 0.02	4
M ($M_\odot$)	1.23 ± 0.15	4
R ($R_\odot$)	2.14 ± 0.05	4
L($L_\odot$)	9.46 ± 0.18	4
Spectral type	F2 V	4

References.—(1) Olsen 1983; (2) ESA 1997; (3) Kaye 1998b; (4) this paper.

4.2. *Photometric Results*

We again used the Vaniček (1971) least-squares method for the frequency analyses of the 718 $V+y$ and 432 B photometric measurements; the results are presented in Table 8. Column (1) lists the photometric bandpass. Column (2) lists the number of observations. Columns (3) and (4) list the resulting periods and corresponding frequencies. Column (5) lists the (peak-to-peak) amplitude. Column (6) lists T_p, a time of photometric minimum near the middle of the data set, assuming each periodicity can be modeled as a pure sine curve.

Figure 5 shows the least-squares spectra of the $V+y$ data set of HD 68192, showing the peaks corresponding to the two periodic signals and their aliases. Both frequencies were confirmed within their errors in the B data set. The residuals shown in the bottom panel of Figure 5 have reached the observational limit of the telescope (3.5 mmag), indicating that no further signals may be detected in this data set.

Figure 6 plots the $V+y$ data phased with the 1.30022 day^{-1} frequency (*top*) and the 1.20220 day^{-1} frequency (*bottom*). The data in the bottom panel have been prewhitened to remove the 1.30022 day^{-1} frequency.

4.3. *Spectroscopic Results*

For HD 68192, the high $v \sin i$ of 85 ± 5 km s^{-1} (Kaye 1998b) resulted in few unblended lines in our blue-wavelength data set. Those lines that remain reasonably

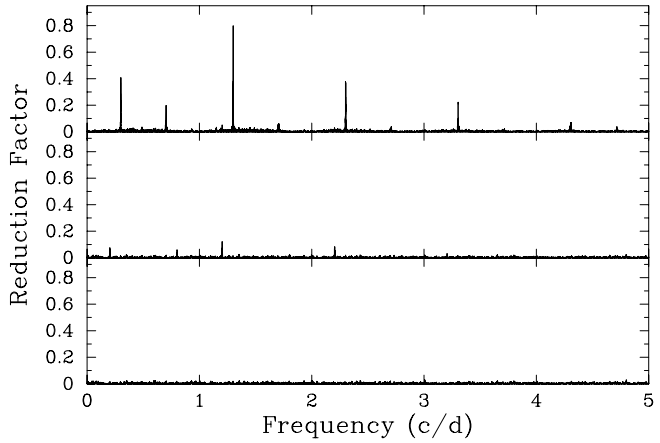

Fig. 5.—Least-squares spectra of the complete $V+y$ data set of HD 68192, showing the two stable periodicities at 1.30022 and 1.20220 day^{-1} and their aliases. Residuals before any signals were treated as known constituents (*top*), after the principal signal was removed (*center*), and after both signals were removed (*bottom*).

TABLE 8

HD 68192: Results from Photometric Data

Photometric Band(s) (1)	n (2)	Period (days) (3)	Frequency (days^{-1}) (4)	Amplitude (mmag) (5)	T_p (HJD − 2,450,000) (6)
$V+y$	718	0.769103 ± 0.000006	1.30022 ± 0.00001	21.7 ± 0.2	834.145 ± 0.002
	718	0.83181 ± 0.00004	1.20220 ± 0.00005	5.4 ± 0.4	834.738 ± 0.022
B	432	0.7691 ± 0.0001	1.3002 ± 0.0002	27.2 ± 0.3	834.142 ± 0.003
	432	0.8319 ± 0.0007	1.2021 ± 0.0010	5.2 ± 0.7	834.719 ± 0.037

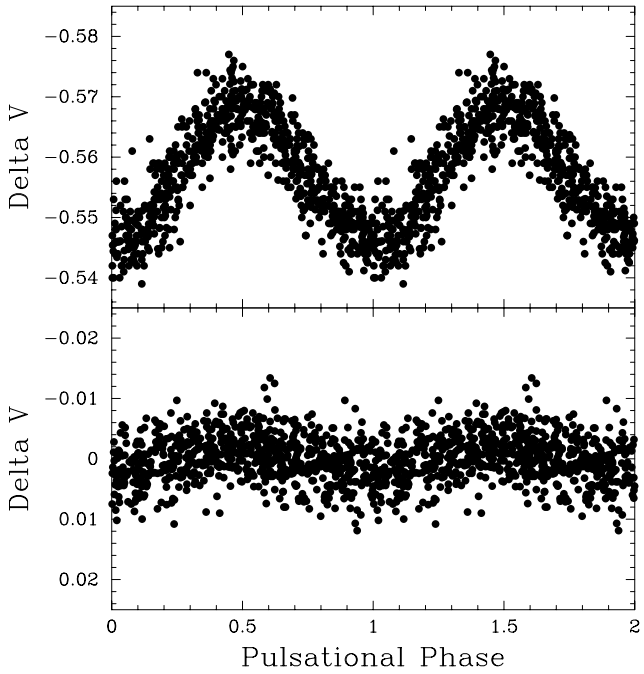

FIG. 6.—The $V+y$ photometric data for HD 68192 phased with the 1.30022 day^{-1} frequency (*top*) and the 1.20220 day^{-1} frequency (*bottom*). The data in the bottom panel have been prewhitened to remove the 1.30022 day^{-1} frequency. Both panels are plotted on the same scale. The time of zero phase corresponds to a time of minimum light, assuming each signal can be modeled as a pure sine curve; HJD = 2,450,834.145 (*top*), HJD = 2,450,834.738 (*bottom*).

blend-free are very shallow. Thus, the method of calculating the first moment of the line profiles with the goal of measuring relative radial velocities did not lend itself to these data. Thus, radial velocities for the 31 KPNO blue-wavelength spectra were computed by assuming that the first spectrum has an arbitrary velocity of zero, and then the other spectra were cross-correlated with the first. Once we obtained the relative radial velocities, we searched them for periodic signals using the method of Vaniĉek (1971).

The power spectrum of the radial velocities of HD 68192 shows a single weak periodicity at a period of 0.70 ± 0.09 days, which is roughly consistent with the principal 0.77 day photometric period. The radial velocity periodicity has a peak-to-peak amplitude of 2.2 ± 0.2 km s^{-1}; the point $V_r = 0$ on the descending portion of the relative radial velocity curve occurs at HJD = 2,450,780.292 ± 0.017 days. Figure 7 shows the relative radial velocity curve phased with this period.

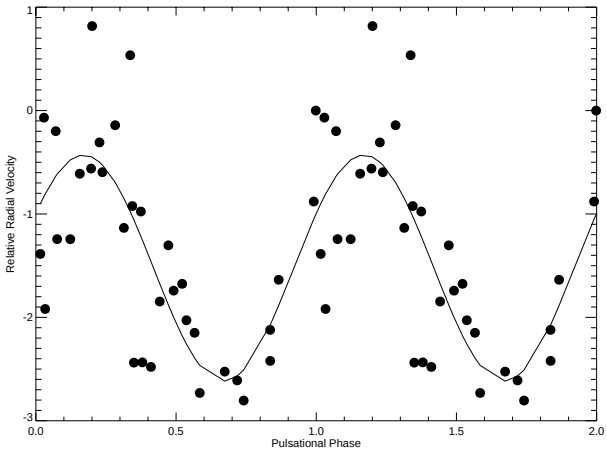

FIG. 7.—Phased relative radial velocity curve for HD 68192 with $\nu = 1.4$ day^{-1} and a time of zero phase of HJD = 2,450,780.292 (*circles*). The line represents the calculated curve.

Velocities from the two additional Na D region observations (the yellow spectra in Table 2) were determined with the IRAF routine RVIDLINES. Each velocity is the mean of the measurement of about six individual lines, including the two Na D lines and additional Fe I features. For HJD = 2,451,260.652 and HJD = 2,451,262.666, we measured velocities of 27.1 and 27.0 km s^{-1}, respectively.

5. DISCUSSION

γ Doradus stars vary in broadband integrated light and are line-profile variables; it is generally agreed that the cause is high-order (n), low-degree (l), nonradial gravity-mode pulsation (see Kaye et al. 1999a and references therein). Since the number of confirmed γ Doradus stars is very small, a careful examination of the available data on each star is crucial to define the γ Doradus instability strip and to understand these stars as a new class of variables.

The basic properties of HD 62454A and HD 68192 (§§ 3.1 and 4.1) reveal both stars to be early F-type main-sequence stars, each falling past the cool edge of the classical δ Scuti instability strip (Fig. 8). Their photometric periods (see §§ 3.2 and 4.2) are too long to be attributed to pressure-mode pulsations found in δ Scuti stars but are consistent with either rotational phenomena or γ Doradus type pulsations.

5.1. *Duplicity Effects*

At least one γ Doradus candidate was dismissed when it was discovered to be an ellipsoidal variable and exhibited no evidence of g-mode pulsations (see Mantegazza & Poretti 1995). Ellipsoidal variables can have periods very similar to those of the high-order, low-degree, nonradial

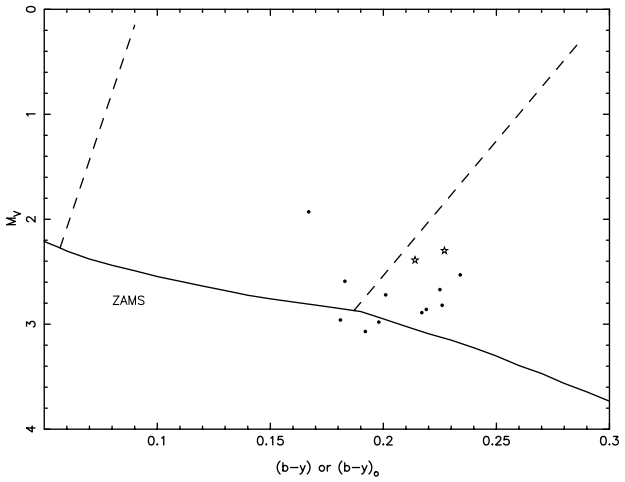

FIG. 8.—Color-magnitude diagram of the bona fide γ Doradus variable stars (see Kaye et al. 1999a and references therein). *Left and right stars*, HD 62454 and HD 68192, respectively; *circles*, others; *solid lines*, zero-age main sequence (Crawford 1975); *dashed lines*, borders of the δ Scuti instability strip (Breger 1979). Courtesy K. Krisciunas. The composite properties of HD 62454 are plotted here since individual measurements of $b-y$ are not available for the two components. HD 62454A, the γ Doradus component, would be located roughly 0.3 mag below the plotted location for the composite star.

gravity-mode pulsations thought to be at work in these objects, and so it is crucial that this mechanism be ruled out.

None of the five photometric periods seen in HD 62454 can be attributed to ellipticity, since they are all much shorter than the 11.615-day orbital period.

If either photometric period in HD 68192 were due to ellipticity, the orbital period would have to be either $1^d.54$ or $1^d.66$, twice the period of photometric variation. Also, the radial velocity amplitude would be many tens of km s^{-1}, unless the orbit were viewed nearly pole-on, but then ellipsoidal variation would not be observed. We showed in § 4.3 (above) that the spectroscopic period is roughly equal to the principal photometric period, and not a factor of 2 longer. In addition, the peak-to-peak amplitude of the V_r variations in HD 68192 are only ~ 2 km s^{-1}. Thus, neither observed photometric period in HD 68192 can arise from the ellipticity effect.

5.2. *Chromospheric Activity*

The last scenario to be dismissed as the cause of γ Doradus variability was the suggestion involving the rotational modulation of starspots (Kaye et al. 1999a). These starspots would cause periodic variations in both the broadband integrated light curves and in the line profiles. They would also have periods similar to those of g-mode pulsations.

HD 62454 shows five simultaneous photometric periods. Using the basic parameters derived for this star (§ 3.1), we estimate an orbital inclination of $i_{\rm orb} \sim 60°$. If the photometric periods are due to the rotation of starspots, our $v \sin i$ value of 11.5 km s^{-1} implies a rotational inclination of $\sim 5°$. If the rotational inclination is $\sim 5°$ (i.e., if the rotational axis and the orbital axis are not aligned), starspots at the equator could perhaps cause the level of variability that we observe. However, at such an inclination, only a narrow (equatorial) band of starspots would be available to cause rotational modulation, and differential rotation could not cause the large observed period range. Therefore, the rotational modulation of any surface features (including starspots) clearly cannot be the cause of the photometric variations observed in HD 62454.

We are also able to argue against the starspot mechanism as the cause of variability in HD 68192 simply by the *stability* of the light variations. The least-squares spectra in Figure 5 are the result of five years of photometric observations, a timescale over which starspots would be born (at some stellar latitude), live (and presumably be redistributed via differential rotation), and die (see, e.g., Henry et al. 1995). The standard deviation of the entire 5 year $V+y$ data set after the removal of the two periodic signals is 0.0035 mag. Therefore, to the precision of our observations, the light curve is indistinguishable from a pair of pure sinusoids, with no changes in amplitude, period, or phase over the entire course of the 5 year data set. Thus, rotational modulation of starspots is not the cause of the observed variations in HD 68192.

5.3. *Concluding Perspective*

Because of the small number of confirmed members of the newly defined γ Doradus variable star class (see Kaye et al. 1999a), HD 62454 and HD 68192 are important additions to the group. Their $b-y$ color and absolute magnitude place them clearly past the cool edge of the classical δ Scuti instability strip (see Fig. 8), where the majority of other γ Doradus stars lie. The amplitude of 5.3 mmag for the 0.83181 day period of HD 68192 is the smallest of any currently known γ Doradus star. HD 62454 is the first bona fide γ Doradus star in a binary system and also has the largest number of g-modes simultaneously detected to date. All of these facts provide valuable constraints on the physical parameters of these new objects.

A. B. K.'s work was performed under the auspices of the US Department of Energy by the Los Alamos National Laboratory under contract W-7405-ENG-36. Astronomy with automated telescopes at Tennessee State University is supported through NASA grant NCC 5-228 and NSF grant HRD 97-06268. We thank the referee for very helpful suggestions, resulting in a significantly improved manuscript. A. B. K. thanks J. A. Guzik, P. A. Bradley, and C. Neuforge for reading various drafts of this manuscript and for helpful conversations.

REFERENCES

Bagnuolo, W. G., Gies, D. R., Hahula, M. E., Wiemker, R., & Wiggs, M. S. 1994, ApJ, 423, 446
Balona, L. A. 1987, MNRAS, 241, 41
Barker, E. S., Evans, D. S., & Laing, J. D. 1967, R. Obs. Bull., 130, 355
Barnes, T. G., Evans, D. S., & Moffett, T. J. 1978, MNRAS, 183, 285
Breger, M. 1979, PASP, 91, 5
Crawford, D. L. 1975, AJ, 80, 955
ESA. 1997, The *Hipparcos* and Tycho Catalogues (ESA SP-1200) (Noorwijk: ESA)
Fekel, F. C. 1997, PASP, 109, 514
Flower, P. J. 1996, ApJ, 469, 355
Gorda, S. Yu., & Svechnikov, M. A. 1998, Astron. Rep., 42, 793
Gray, D. F. 1992, The Observation and Analysis of Stellar Photospheres (Cambridge: Cambridge Univ. Press)
Gray, R. O. 1998, AJ, 116, 482
Gray, R. O., Graham, P. W., & Hoyt, S. R. 1999, in preparation
Guzik, J. A., Kaye, A. B., & Bradley, P. A. 1999, in preparation
Henry, G. W. 1995, in ASP Conf. Ser. 79, Robotic Telescopes: Current Capabilities, Present Developments, and Future Prospects for Automated Astronomy, ed. G. W. Henry & M. Drummond (San Francisco: ASP), 44
Henry, G. 1999, PASP, 111, 845
Henry, G. W., Eaton, J. A., Hamer, J., & Hall, D. S. 1995, ApJS, 97, 513
Kaye, A. B. 1998a, Inf. Bull. Variable Stars, No. 4596
———. 1998b, Ph.D. thesis, Georgia State Univ.
Kaye, A. B., Handler, G. W., Krisciunas, K., Poretti, E., & Zerbi, F. M. 1999a, PASP, 111, 840
Kaye, A. B., Henry, G. W., Fekel, F. C., & Hall, D. S. 1999b, MNRAS, in press
Krisciunas, K., Crowe, R. A., Luedeke, K. D., & Roberts, M. 1995, MNRAS, 277, 1404
Kurucz, R. L. 1993, ATLAS9 Stellar Atmosphere Programs and 2 km/s Grid (Cambridge: Smithsonian Astrophys. Obs.)
Mantegazza, L., & Poretti, E. 1995, A&A, 294, 190
Olsen, E. H. 1983, A&AS, 54, 55
Penny, L. R., Gies, D. R., & Bagnuolo, W. G., Jr., 1997, ApJ, 483, 439
Scarfe, C. D., Batten, A. H., & Fletcher, J. M. 1990, Publ. Dom. Astrophys. Obs. Victoria, 18, 21
Vaniček, P. 1971, Ap&SS, 12, 10
Zerbi, F. M., et al. 1999, MNRAS, 303, 275